Supporting Information

Tunable Axial Symmetry β-ketoamine Covalent Organic Frameworks for Efficient Photocatalytic H_2O_2 Synthesis in Seawater

Jinyang Chen, [a, c†] Jie Zhou, [a, b†] Na Li, [a] Yeshun Liu, [a] Xubing Deng, [a] Faliang Gou, [a] Zhen Yang, [a] Minfeng Zeng, *[a] Mingchao Shao, *[b,c] and Yunlong Guo*[c]

[a] Zhejiang Key Laboratory of Alternative Technologies for Fine Chemicals Process, College of Chemistry & Chemical Engineering, Shaoxing University, Shaoxing 312000, P. R. China. Shaoxing 312000, P. R. China.

[b] State Key Laboratory of Solid Lubrication, Lanzhou Institute of Chemical Physics, Chinese Academy of Sciences, Lanzhou 730000, P. R. China.

[c] Beijing National Laboratory for Molecular Sciences, Organic Solids Laboratory, Institute of Chemistry, Chinese Academy of Sciences, Beijing 100190, P. R. China.

* Corresponding Author. Email: zengmf@usx.edu.cn; shaomingchao@licp.cas.cn; guoyunlong@iccas.ac.cn

[†]These authors contributed equally to this work and should be considered co-first authors.

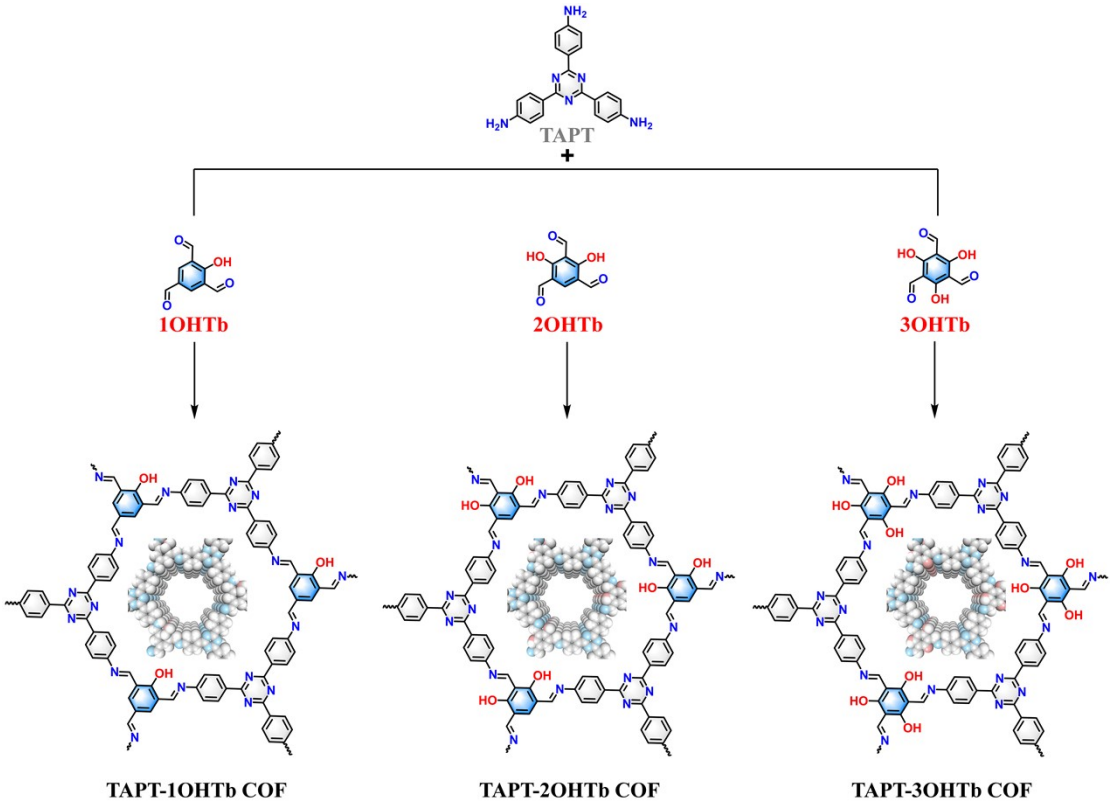

Scheme S1. Schematic diagram of the synthesis route and chemical structure of TAPT-1OHTb COF, TAPT-2OHTb COF, and TAPT-3OHTb COF.

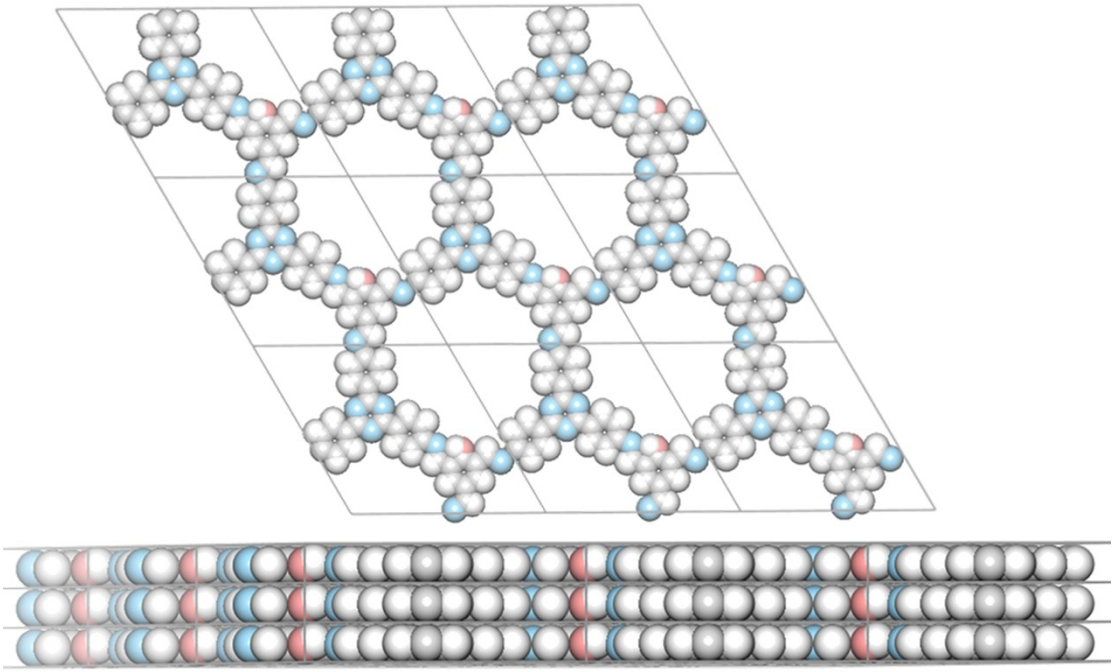

Fig. S1. Simulated molecular structure of TAPT-1OHTb COF with AA stacking (Cell parameters: a =18.80 Å, b = 18.62 Å, c = 3.44 Å, α = β = 90°, γ = 120°).

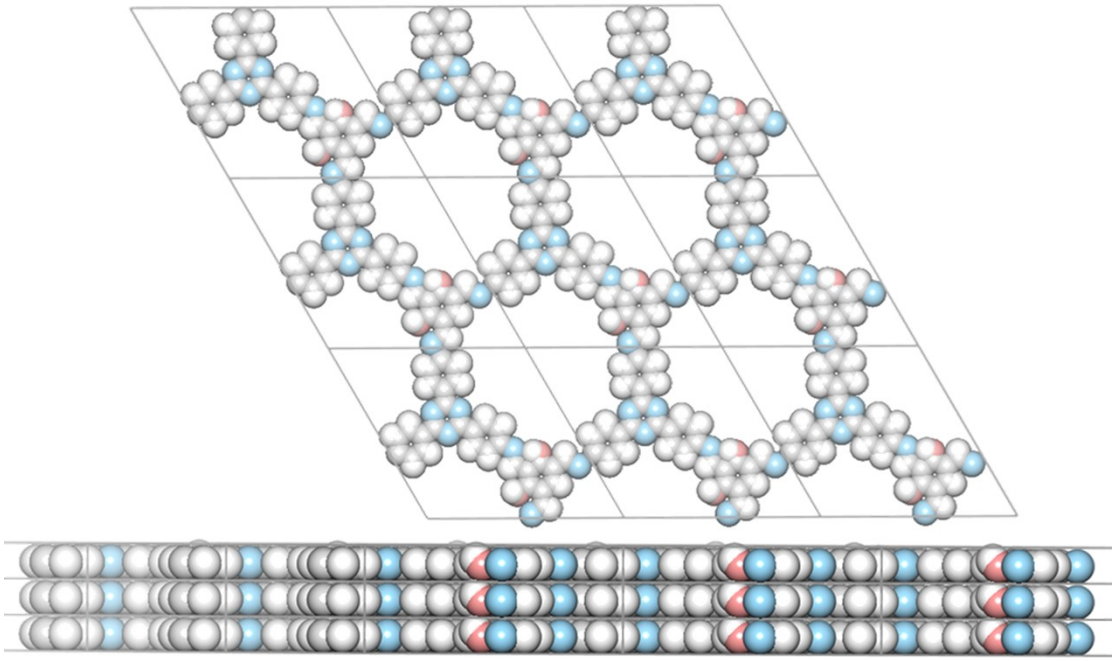

Fig. S2. Simulated molecular structure of TAPT-2OHTb COF with AA stacking (Cell parameters: a =18.70 Å, b = 18.67Å, c = 3.45 Å, α = β = 90°, γ = 120°).

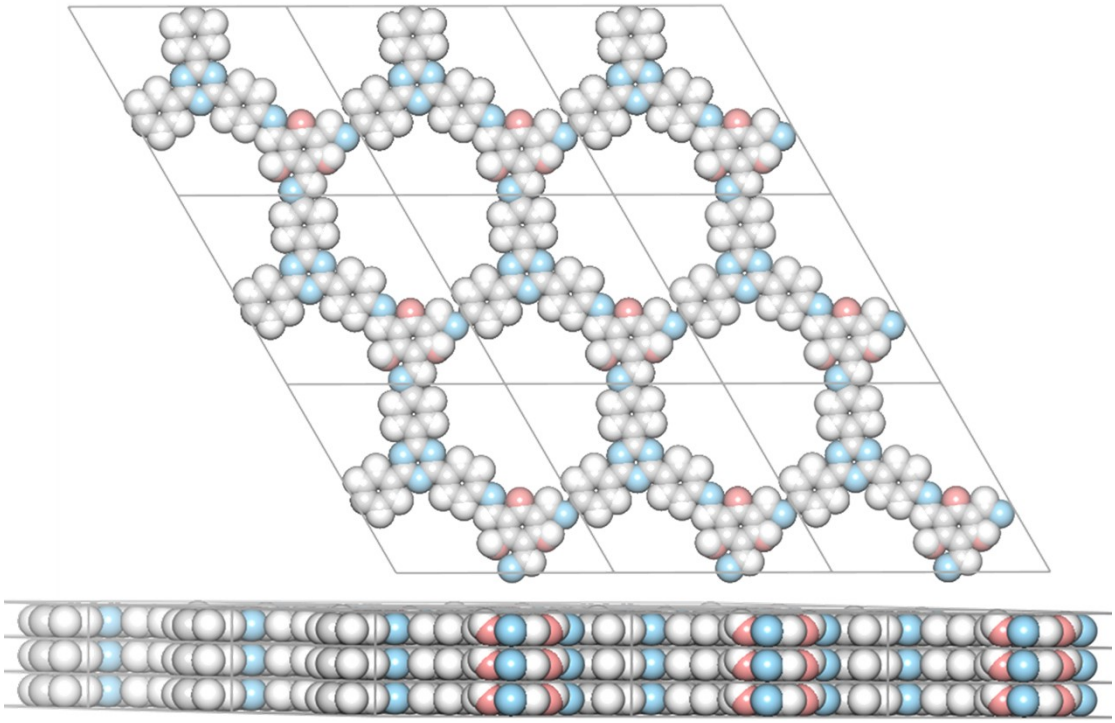

Fig. S3. Simulated molecular structure of TAPT-3OHTb COF with AA stacking. (Cell parameters: a =18.68 Å, b = 18.70Å, c = 3.47 Å, α = β = 90°, γ = 120°).

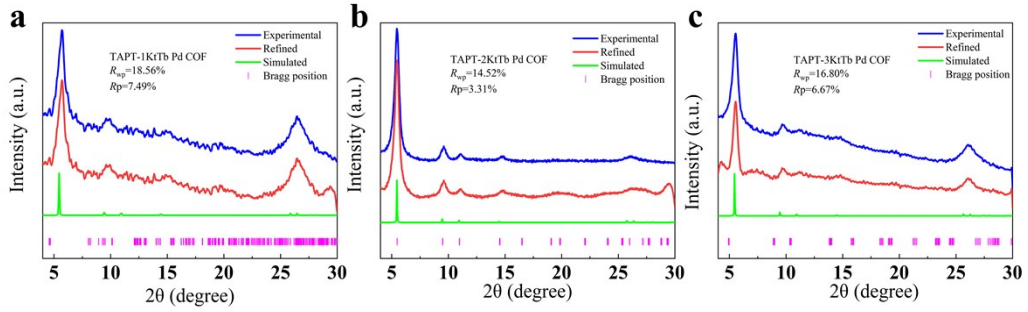

Fig. S4. Pawley refinement of the PXRD pattern of (a) TAPT-1KtTb Pd COF, (b) TAPT-2KtTb Pd COF, and (c) TAPT-3KtTb Pd COF.

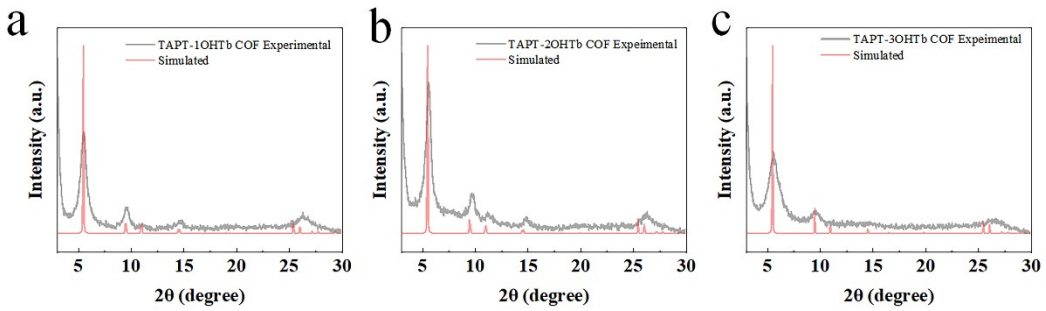

Fig. S5. The PXRD pattern of (a) TAPT-1OHTb COF, (b) TAPT-2OHTb COF, and (c) TAPT-3OHTb COF.

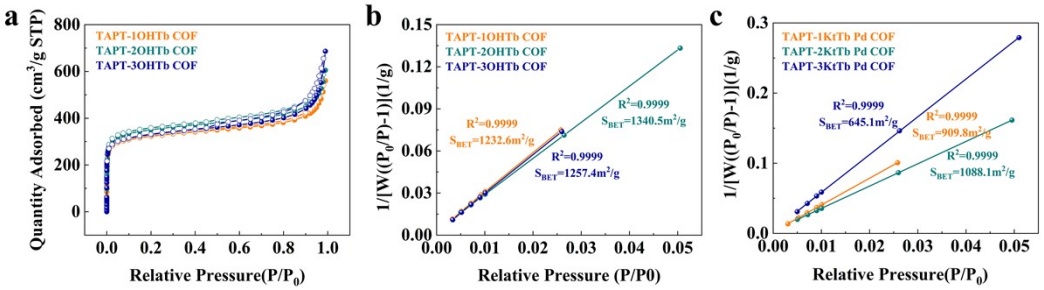

Fig. S6. (a) N_2 adsorption and desorption isotherm of pure COF materials. (b) The specific surface area of pure COF materials. (c) The specific surface area of containing metal Pd COF materials.

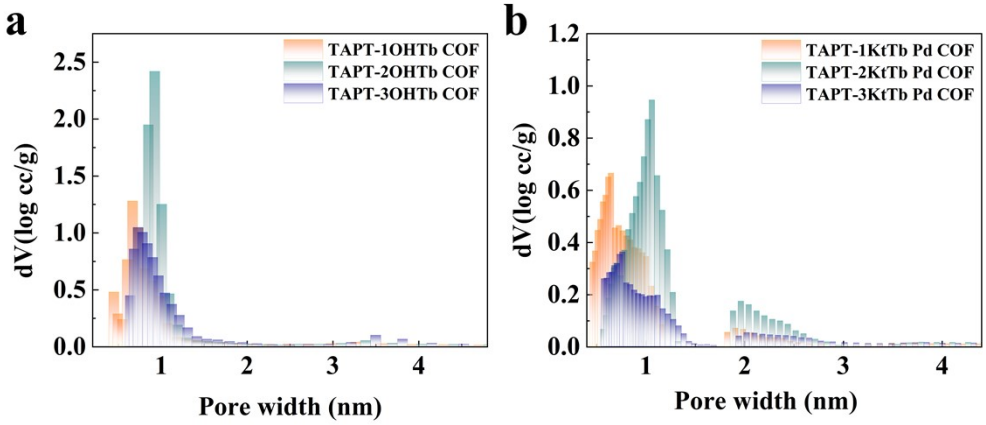

Fig. S7. Pore size distribution of materials (a) without metal Pd COFs and (b) containing metal Pd COFs.

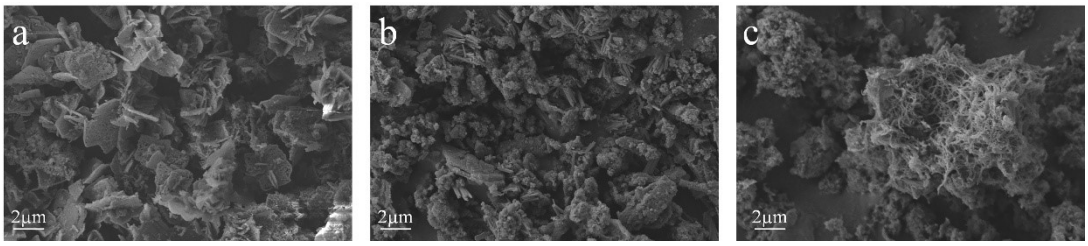

Fig. S8. SEM images of (a) TAPT-1KtTb Pd COF, (b) TAPT-2KtTb Pd COF, and (c) TAPT-3KtTb Pd COF. Ruler size: 2μm

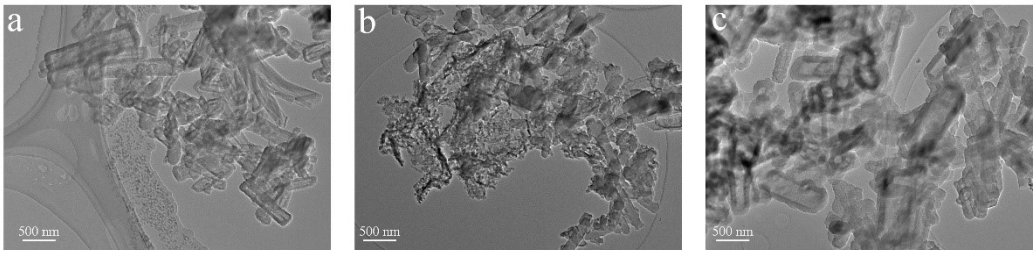

Fig. S9. HRTEM images of (a) TAPT-1KtTb Pd COF, (b) TAPT-2KtTb Pd COF, and (c) TAPT-3KtTb Pd COF. Ruler size: 500nm.

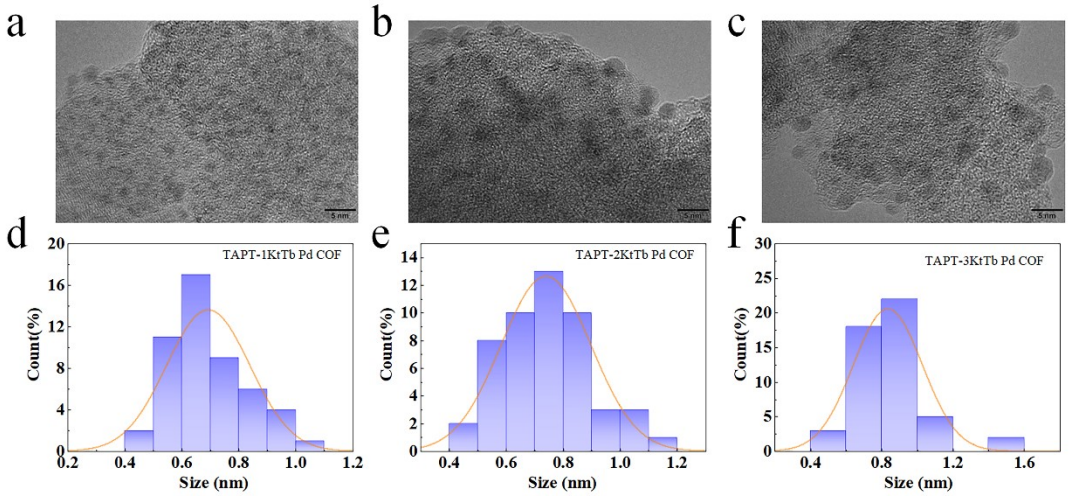

Fig. S10. HRTEM image of (a) TAPT-1KtTb Pd COF, (b) TAPT-2KtTb Pd COF, and (c) TAPT-3KtTb Pd COF, Particle size distribution of (d) TAPT-1KtTb Pd COF, (e) TAPT-2KtTb Pd COF, and (f) TAPT-3KtTb Pd COF.

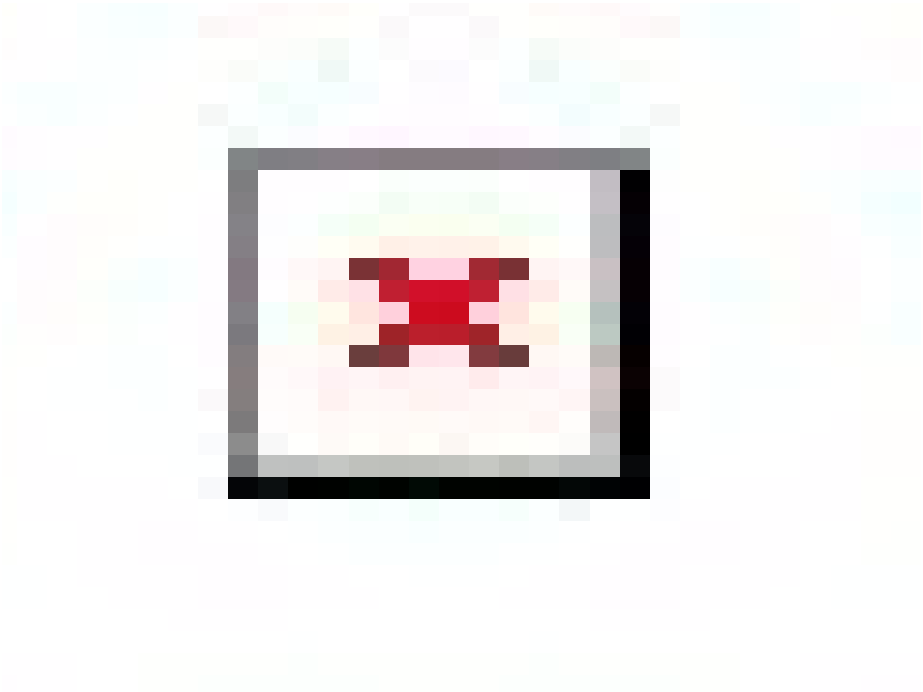

Fig. S11. The solid-state ^{13}C NMR spectra of TAPT-1OHTb COF, TAPT-2OHTb COF, and TAPT-3OHTb COF.

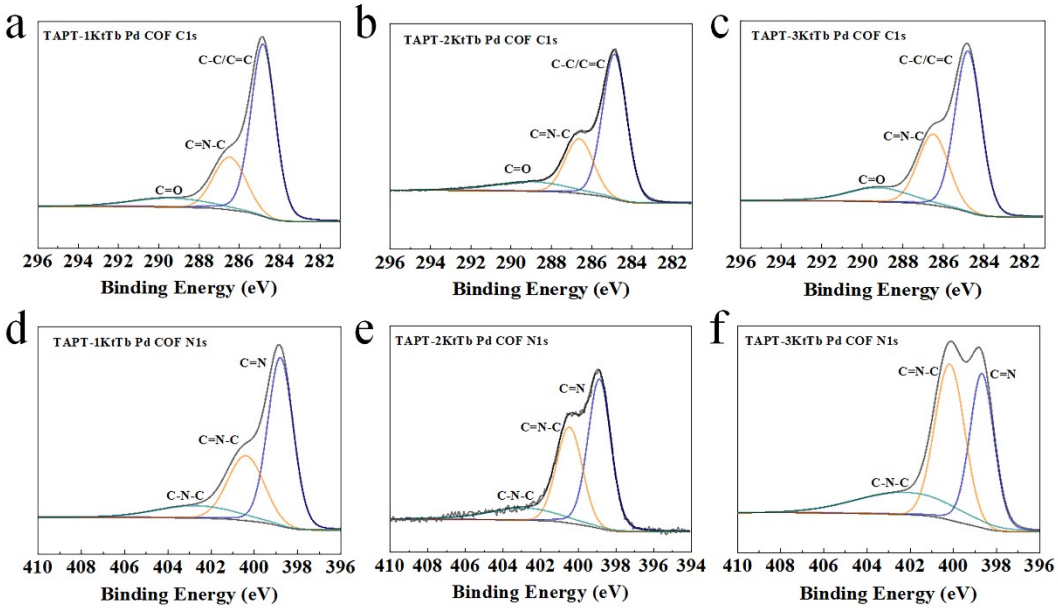

Fig. S12. C1s XPS spectra of (a) TAPT-1KtTb Pd COF, (b) TAPT-2KtTb Pd COF, and (c) TAPT-3KtTb Pd COF, N1s XPS spectra of (d) TAPT-1KtTb Pd COF, (e) TAPT-2KtTb Pd COF, and (f) TAPT-3KtTb Pd COF.

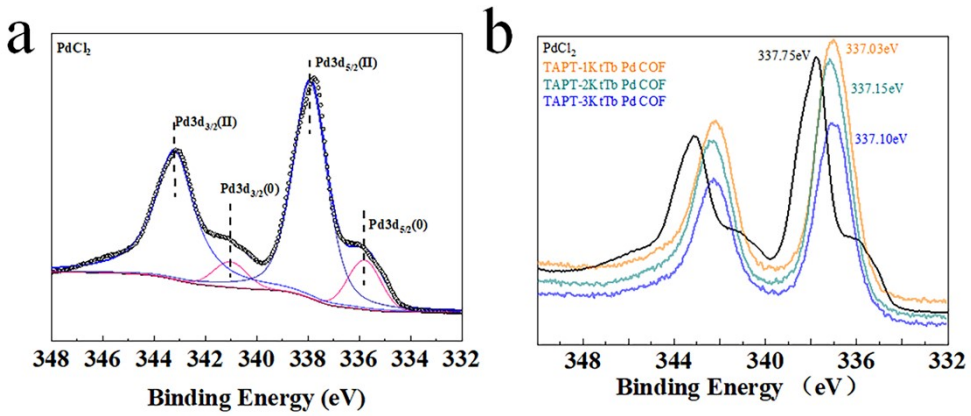

Fig. S13. (a) XPS spectra of Pd species in $PdCl_2$, (b) XPS spectra of three COFs locked with Pd species. The Pd3d binding energy moved towards the low field, indicating an interaction between the Pd species and COF.

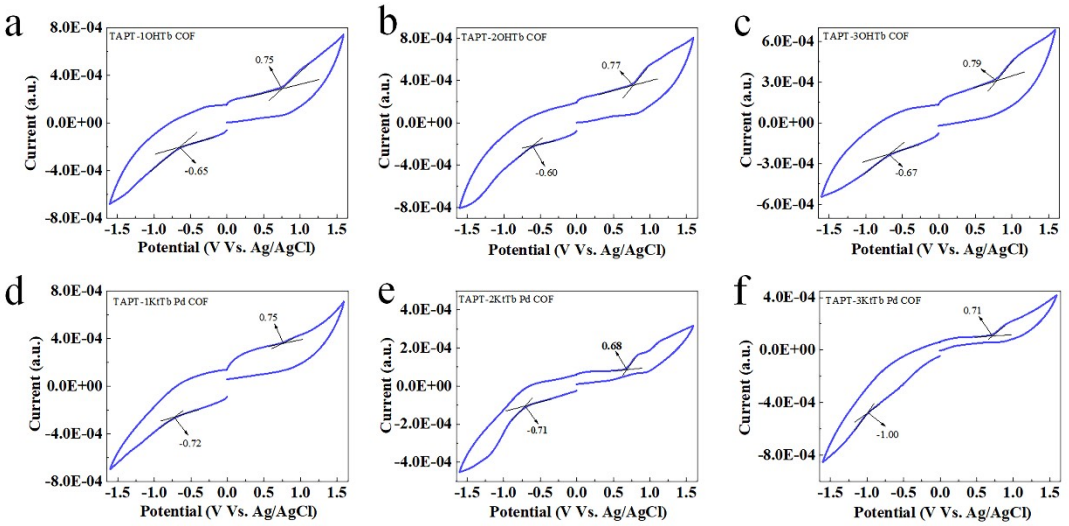

Fig. S14. Cyclic voltammetry determination of band structure of three COFs materials and after Pd locked materials.

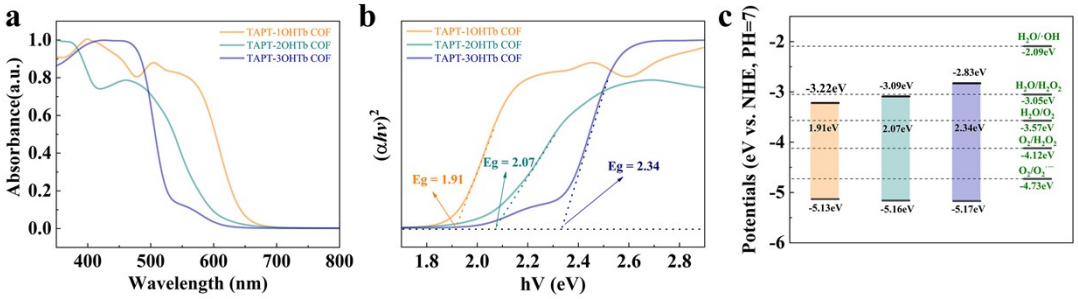

Fig. S15. (a) UV-Vis spectra illustrate the absorption characteristics of the COFs in response to light. (b) Tauc plots provide insights into the bandgap energy distribution. (c) Band structure diagrams reveal the arrangement of electronic energy levels (TAPT-1KtTb Pd COF: yellow, TAPT- 2KtTb Pd COF: green, TAPT- 3KtTb Pd COF: blue,).

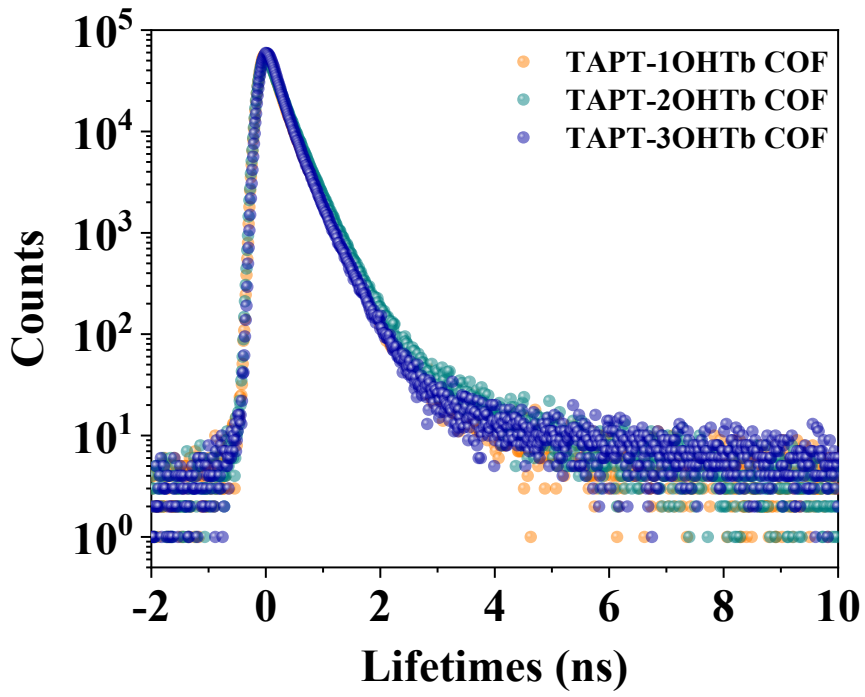

Fig. S16. The positron annihilation analysis of TAPT-1OHTb COF, TAPT-2OHTb COF, and TAPT-3OHTb COF.

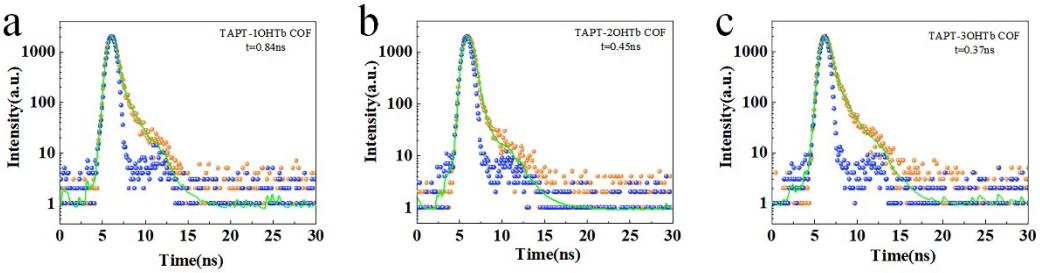

Fig. S17. Fluorescence lifetime spectra of three COF materials.

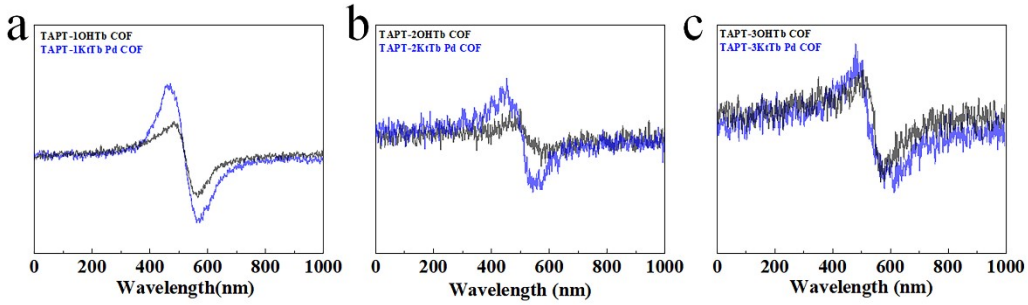

Fig. S18. EPR spectra of three COF materials.

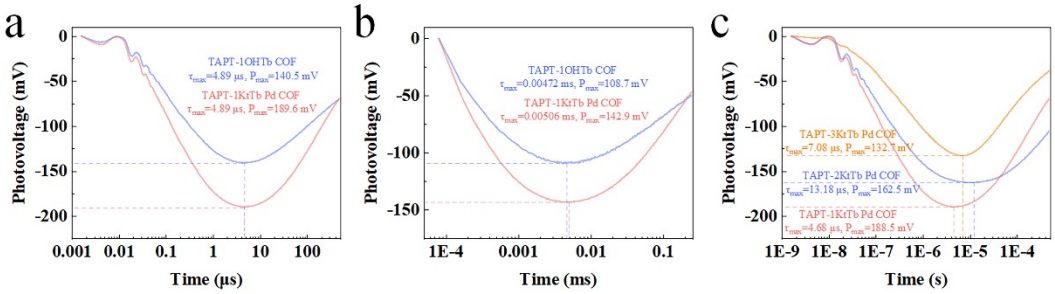

Fig. S19. TPV spectra of COF materials.

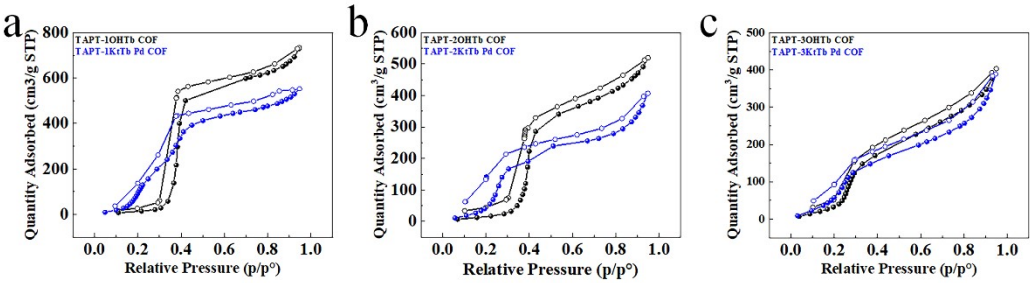

Fig. S20. Water vapor adsorption tests of three COFs materials and after Pd locked materials.

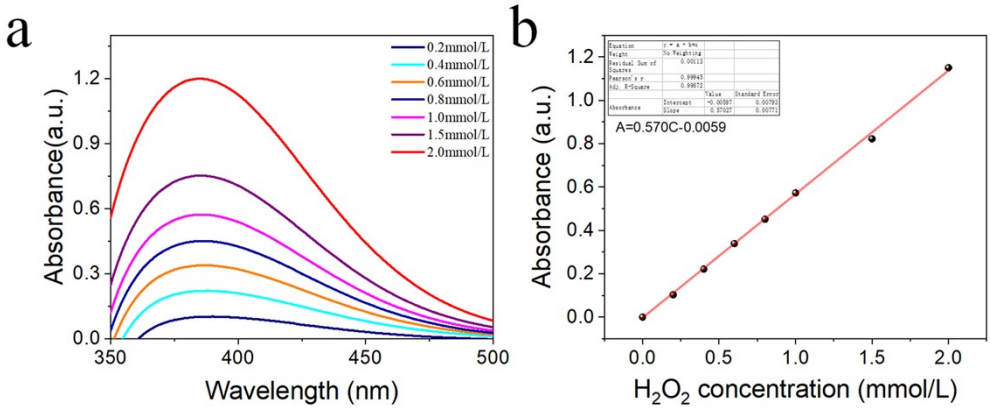

Fig. S21. Absorbance and standard curve plot of H_2O_2.

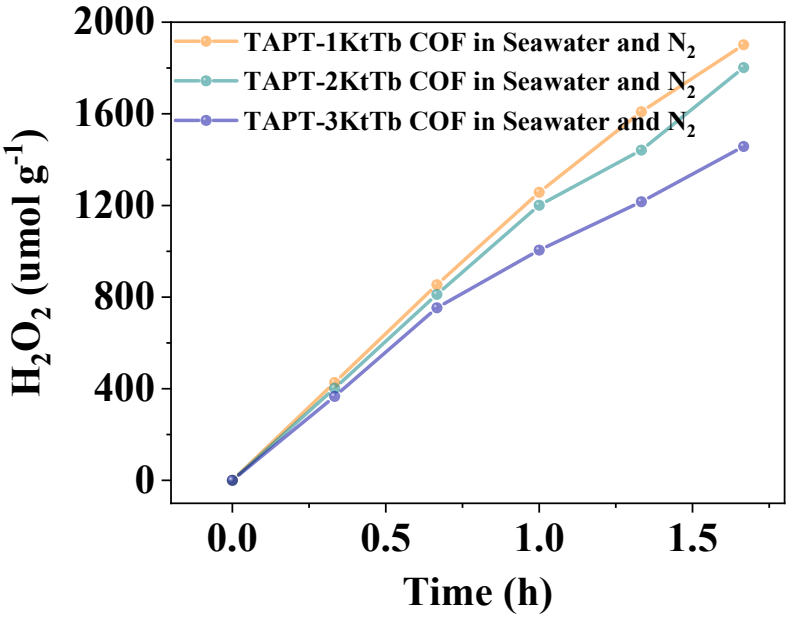

Fig. S22. Photocatalytic H_2O_2 production rate in seawater under N_2 atmospheres.

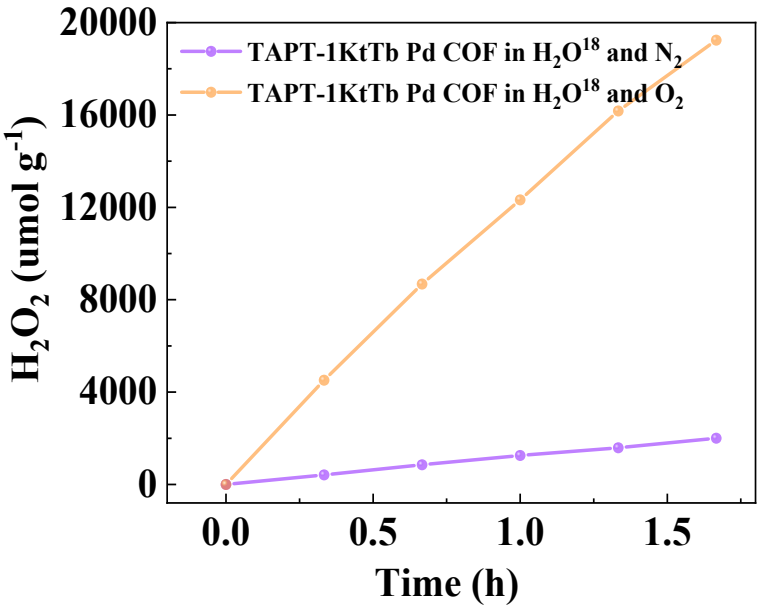

Fig. S23. Photocatalytic H_2O_2 production rate in H_2O^{18} under O_2/N_2.

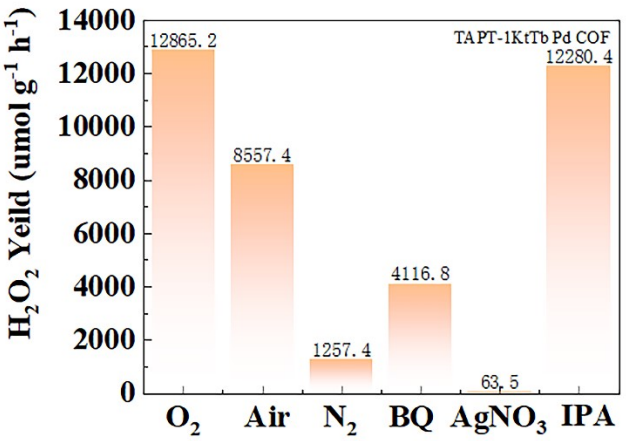

Fig. S24. Free radical quenching and trapping experiments. P-benzoquinone (BQ) was used as the O_2^- quencher, isopropyl alcohol (IPA) was used as the OH quenching agent, and silver nitrate was used as the electron (e-) quenching agent. The results show that adding BQ, the yield of H_2O_2 decreased by 68%; There was no significant change in yield after adding IPA; After adding silver nitrate, the yield basically disappears. It was shown that $\bullet O_2^-$ was the main active species, consistent with the results of in situ FTIR and in situ EPR, confirming that the reaction followed "$O_2+2e^- +2H^+ \rightarrow H_2O_2$ and $O_2+e^- \rightarrow \bullet O_2^-$, $\bullet O_2^- +e^- +2H^+ \rightarrow H_2O_2$", one-step $2e^-$ and two-step $1e^-$ path mechanisms.

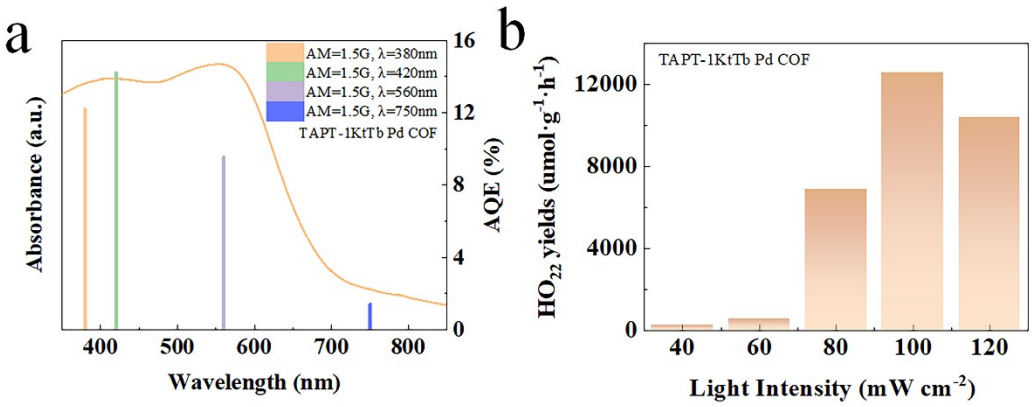

Fig. S25. (a) Apparent quantum efficiency at different visible light wavelengths, (b) Photocatalytic performance at different irradiation intensities at 420nm.

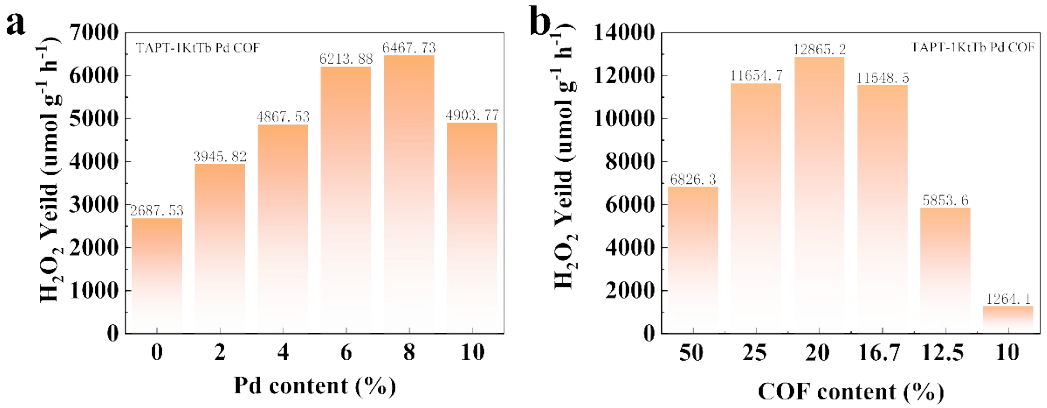

Fig. S26. Photocatalytic production of H_2O_2 under different Pd content and COFs content.

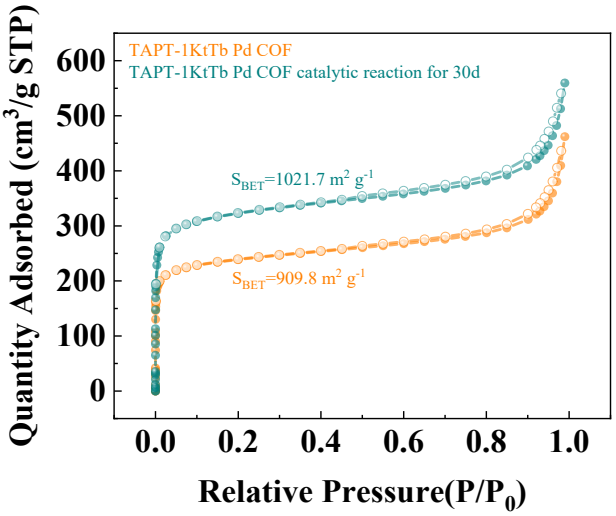

Fig. S27. N_2 sorption isotherms for characterizing the porosity and surface area after photocatalytic cycled for one month.

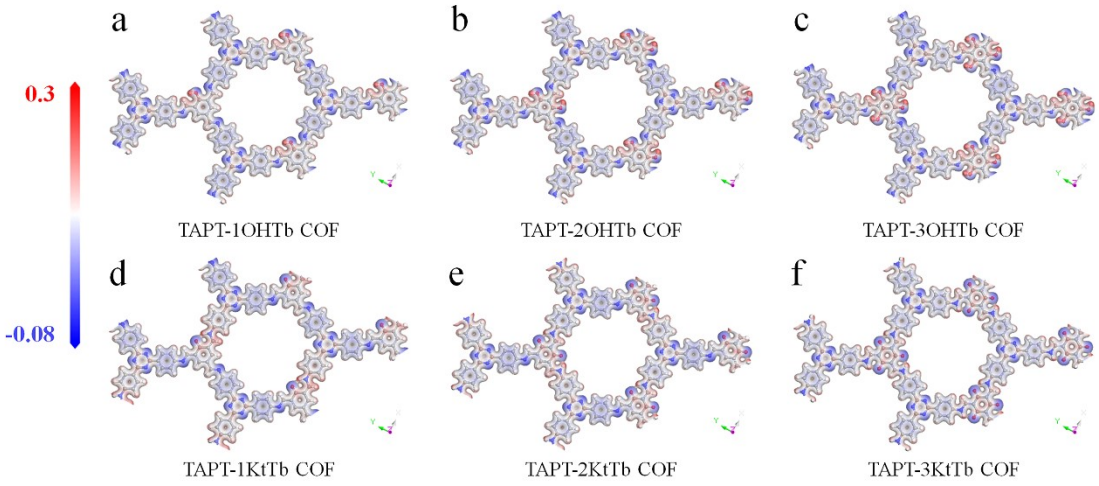

Fig. S28. Electron cloud density of a single complete molecular structure.

Table S1. The ICP results of palladium content on TAPT-1KtTb Pd COF, TAPT-2KtTb Pd COF and TAPT-3KtTb Pd COF.

Sample	Pd (%)
TAPT-1KtTb Pd COF	6.6
TAPT-2KtTb Pd COF	6.7
TAPT-3KtTb Pd COF	6.5

Table S2. The BET results of TAPT-1KtTb Pd COF, TAPT-2KtTb Pd COF, and TAPT-3KtTb Pd COF.

Sample	S_{BET} ($m^2\ g^{-1}$)	V ($cm^3\ g^{-1}$)	L_{DFT} (nm)
TAPT-1OHTb COF	1232.6	0.748	0.785
TAPT-2OHTb COF	1340.5	0.836	1.178
TAPT-3OHTb COF	1257.4	0.571	0.590
TAPT-1KtTb Pd COF	909.8	0.561	0.704
TAPT-2KtTb Pd COF	1088.1	0.681	1.061
TAPT-3KtTb Pd COF	645.1	0.504	0.704

Table S3. The positron annihilation analysis of COFs.

Sample	τ_1(ns)	τ_2(ns)	τ_3(ns)	τ_4(ns)	$l_{(\tau3)}$ (nm)	$R_{(\tau4)}$ (nm)	$d_{(\tau4)}$ (nm)
TAPT-1OHTb COF	0.15	0.31	1.27	12.1	0.205	0.711	1.422
TAPT-2OHTb COF	0.19	0.33	1.33	11.6	0.213	0.698	1.397
TAPT-3OHTb COF	0.16	0.31	1.69	9.7	0.254	0.646	1.291
TAPT-1KtTb Pd COF	0.17	0.33	1.53	6.2	0.237	0.526	1.052
TAPT-2KtTb Pd COF	0.18	0.33	1.51	8.9	0.235	0.621	1.243
TAPT-3KtTb Pd COF	0.16	0.32	1.82	7.9	0.268	0.589	1.177

Table S4. Comparisons of H_2O_2 production rates, SCC, and AQE by COF-based photocatalysts.

Samples	**Irradiation conditions**	**Reaction environment**	**H_2O_2 yields ($\mu mol \cdot g^{-1} \cdot h^{-1}$)**	**AQE %**	**SCC %**	**Ref.**
TAPT-1KtTb Pd COF	λ＞420nm	Seawater, O_2	12865.2	14.2	2.09	**This work**
TAPT-1KtTb Pd COF	λ＞420nm	Seawater, Air	8557.4	10.5	1.39	**This work**
TAPT-2KtTb Pd COF	λ＞420nm	Seawater, O_2	9512.5	11.4	1.54	**This work**

TAPT-2KtTb Pd COF	λ＞420nm	Seawater, Air	6351.3	6.9	1.03	**This work**
TAPT-3KtTb Pd COF	λ＞420nm	Seawater, O_2	7789.4	8.2	1.27	**This work**
TAPT-3KtTb Pd COF	λ＞420nm	Seawater, Air	5625.2	5.7	0.91	**This work**
TT-COF	λ=400-700 100mW/cm^2	Seawater, Air	2890	---	0.14 %	[1]
TD-COF	λ=400-700 100mW/cm^2	Seawater, Air	3364	---	0.15 %	[1]
TA-COF	λ=400-700 100mW/cm^2	Seawater, Air	1640	---	---	[2]
TB-COF	λ=400-700 100mW/cm^2	Seawater, Air	4111	3.45 %	1.08 %	[2]
TiO_2 QDs/g-C_3N_4	λ=440	Seawater, O_2	1172	11.2 %	---	[3]
PM-CDs	λ≥440	Seawater, O_2	1776	1.25 %	0.21 %	[4]
TPT-COF	λ=420	Seawater, O_2	4006	---	---	[5]
TPB-COF	λ=420	Seawater, O_2	5696	---	---	[5]
3D-GCN-T	λ=412 90mW/cm^2	Simulated seawater, Air	800	17%	---	[6]
UP-TP	AM1.5G	Seawater, O_2	3846	4.5%	---	[7]
PTTN-AO	AM1.5G	Seawater, O_2	3000	---	---	[8]
TBA-COF	λ=420	Seawater, O_2	8878	---	0.62 %	[9]
TCA-COF	λ=420	Seawater, O_2	6023	---	0.42 %	[9]
COF-1	λ＞420nm	Seawater, Air	4416	---	---	[10]
COF-2	λ＞420nm	Seawater, Air	6930	---	---	[10]

Table S5. Relevant DFT calculation data of COFs with different types and different symmetrical structures.

Sample	**|Total Energy| (eV)**	**HOMO (eV)**	**LUMO (eV)**	***Eg* (eV)**	
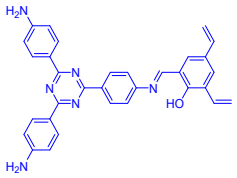	**44575.27**	**-4.44**	**-2.45**	**1.99**	**This work**
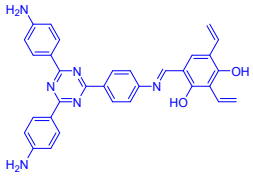	**46621.88**	**−4.77**	**−2.40**	**2.07**	**This work**
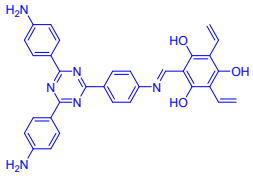	**48668.72**	**−4.49**	**−2.24**	**2.25**	**This work**
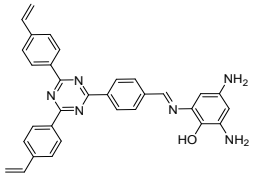	44574.98	−3.65	−2.60	1.05	COFs1
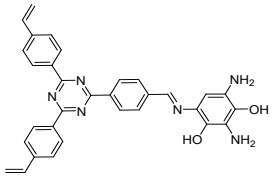	46621.83	−3.94	−2.63	1.31	COFs1
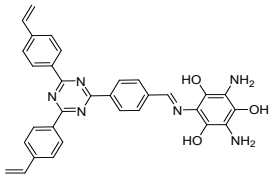	48668.65	−3.86	−2.55	1.31	COFs1
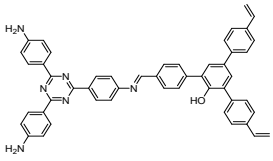	63428.06	−4.32	−2.40	1.92	COFs2

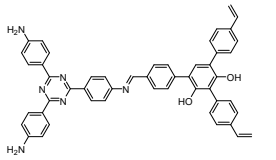	65474.13	−4.42	−2.46	1.96	COFs2
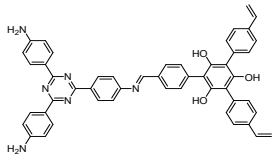	67521.65	−4.34	−2.22	2.11	COFs2
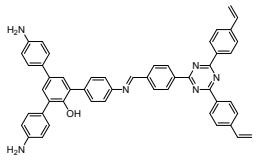	63427.86	−3.78	−2.69	1.11	COFs3
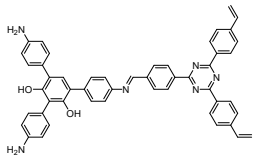	65474.61	−3.74	−2.62	1.12	COFs3
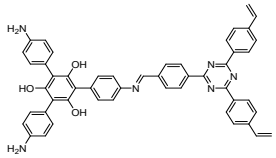	67521.47	−3.78	−2.63	1.15	COFs3
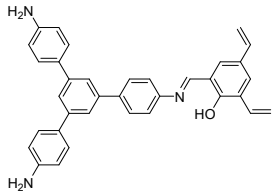	43265.12	−4.06	−2.29	1.77	COFs4
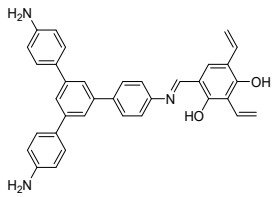	45312.04	−4.04	−2.18	1.86	COFs4
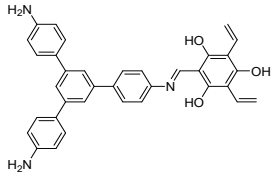	47358.95	−4.01	−2.10	1.91	COFs4

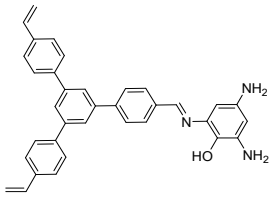	43264.90	−3.55	−2.12	1.43	COFs5
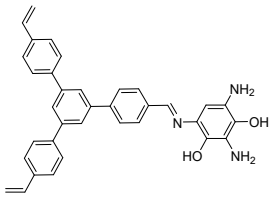	45311.44	−3.83	−2.21	1.62	COFs5
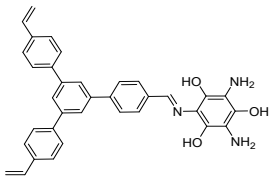	47357.96	−3.75	−2.11	1.64	COFs5
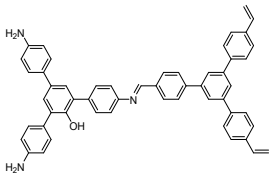	62117.76	−3.74	−2.22	1.52	COFs6
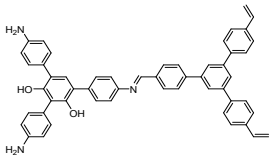	64164.60	−3.69	−2.14	1.55	COFs6
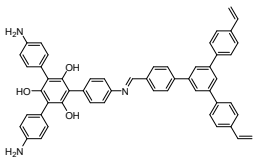	66211.34	−3.72	−2.13	1.59	COFs6
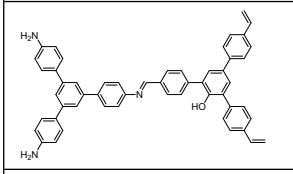	62117.70	−4.04	−2.27	1.77	COFs7
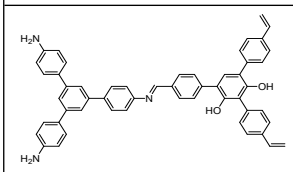	64164.45	−4.02	−2.21	1.81	COFs7

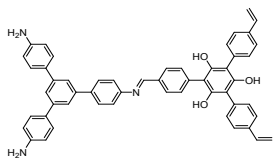	66211.28	−4.00	−2.11	1.89	COFs7
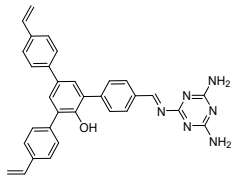	44575.31	−4.55	−2.53	2.02	COFs8
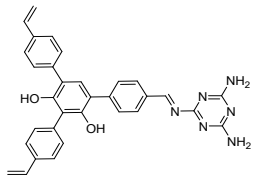	46621.85	−4.44	−2.40	2.04	COFs8
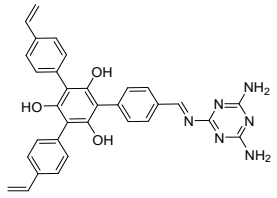	48668.36	−4.58	−2.47	2.11	COFs8
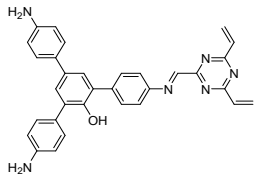	44574.10	−3.86	−2.86	1.00	COFs9
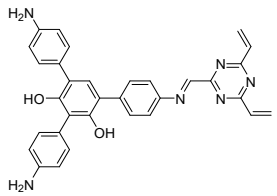	46620.98	−4.03	−2.84	1.19	COFs9
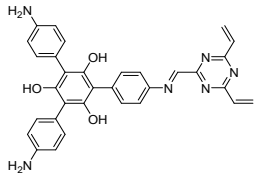	48667.72	−4.17	−2.84	1.33	COFs9

References

[1] J.-Y. Yue, L.-P. Song, Y.-F. Fan, Z.-X. Pan, P. Yang, Y. Ma, Q. Xu, B. Tang, Thiophene-Containing Covalent Organic Frame-works for Overall Photocatalytic H_2O_2 Synthesis in Water and Seawater. Angew. Chem. Int. Ed. 62 (2023) e202309624, https://doi.org/10.1002/anie.202309624.

[2] J.-Y. Yue, L.-P. Song, Z.-X. Pan, P. Yang, Y. Ma, Q. Xu, B. Tang, Regulating the H_2O_2 Photosynthetic Activity of Covalent Organic Frameworks through Linkage Orientation. ACS Catal. 14 (2024) 4728-4737, https://doi.org/10.1021/acscatal.4c00278.

[3] H. Zhang, S. Wang, J. Tian, X. Bai, Photocatalytic hydrogen peroxide production from seawater over graphitic carbon nitride supported titanium dioxide quantum dots. J. Environ. Chem. Eng. 12 (2024) 112290, https://doi.org/10.1016/j.jece.2024.112290.

[4] Q. Wu, J. Cao, X. Wang, Y. Liu, Y. Zhao, H. Wang, Y. Liu, H. Huang, F. Liao, M. Shao, Z. Kang, A metal-free photocatalyst for highly efficient hydrogen peroxide photoproduction in real seawater. Nat Commun. 12 (2021) 483, https://doi.org/10.1038/s41467-020-20823-8.

[5] J.-Y. Yue, L.-P. Song, Z.-X. Pan, M. Cheng, X. Wang, Q. Xu, P. Yang, Overall solar H_2O_2 generation in water and real seawater by covalent organic frameworks with kgd topology. Chem. Eng. J. 504 (2025) 158983, https://doi.org/10.1016/j.cej.2024.158983.

[6] R.A. Borges, M.F. Pedrosa, Y.A. Manrique, C.G. Silva, A.M.T. Silva, J.L. Faria, M.J. Sampaio, 3D structured photocatalysts for sustainable H_2O_2 generation from saccharides derivatives. Chem. Eng. J. 470 (2023) 144066, https://doi.org/10.1016/j.cej.2023.144066.

[7] X. Shi, Y. You, L. Huang, J. Zhao, W. Ji, L. Li, D. Bu, S. Huang, Interfacial

Engineering of β-Ketoenamine-Based COFs/Urea-Linked Perylene Diimide for Overall Photosynthesis of H_2O_2 in Seawater. Adv. Funct. Mater. 35 (2025) 2414755, https://doi.org/10.1002/adfm.202414755.

[8] Z. Yu, F. Yu, M. Xu, S. Feng, J. Qiu, J. Hua, Amidoxime-Functionalized sp^2-Carbon-Conjugated Covalent Organic Frameworks for Overall Photocatalytic Hydrogen Peroxide Production. Adv. Sci. 12 (2025) 2415194, https://doi.org/10.1002/advs.202415194.

[9] J.-Y. Yue, Z.-X. Pan, R.-Z. Zhang, Q. Xu, P. Yang, B. Tang, One-Pot Synthesis of Fully Conjugated Covalent Organic Frameworks via the Pictet–Spengler Reaction for Boosting H_2O_2 Photogeneration in Real Seawater. Adv. Funct. Mater. 35 (2025) 2421514, https://doi.org/10.1002/adfm.202421514.

[10] Y. Xie, F. Mao, Q. Rong, X. Liu, M. Hao, Z. Chen, H. Yang, G.I.N. Waterhouse, S. Ma, X. Wang, Rational Design of 3D Space Connected Donor–Acceptor System in Covalent Organic Frameworks for Enhanced Photocatalytic Performance. Adv. Funct. Mater. 34 (2024) 2411077, https://doi.org/10.1002/adfm.202411077.